Chapter 24
Failure Simulations with a Strain Rate Dependent Ductile-to-Brittle Transition Model

Juha Hartikainen, Kari Kolari, and Reijo Kouhia

Abstract In this paper, simulations with a phenomenological model to describe the ductile-to-brittle transition of rate-dependent solids are presented. The model is based on consistent thermodynamic formulation using proper expressions for the Helmholtz free energy and the dissipation potential. In the model, the dissipation potential is additively split into damage and visco-plastic parts and the transition behaviour is obtained using a stress dependent damage potential. The damage is described by using a vectorial variable.

Keywords Constitutive model · Continuum damage mechanics · Viscoplasticity · Dissipation potential · Ductile-to-brittle transition

24.1 Introduction

Most materials exhibit rate-dependent inelastic behaviour. An increasing strain rate usually increases the yield stress thus enlarging the elastic range. However, the ductility is gradually lost and for some materials there exists a rather sharp transition strain rate zone after which the material behaviour is completely brittle.

In this paper, a phenomenological approach to model the ductile-to-brittle transition of rate-dependent solids is presented. It is an extension to the model presented in [1, 5] using a vectorial damage variable [8]. The model is based on consistent thermodynamic formulation using proper expressions for the Helmholtz free energy and dissipation potential. The dissipation potential is additively split into damage

J. Hartikainen (✉)
Aalto University, P.O. Box 12100, 00076 Aalto, Finland
e-mail: juha.hartikainen@aalto.fi

K. Kolari
VTT, P.O. Box 1000, 02044 VTT, Finland
e-mail: kari.kolari@vtt.fi

R. Kouhia
Tampere University of Technology, P.O. Box 589, 33101 Tampere, Finland
e-mail: reijo.kouhia@tut.fi

S. Repin et al. (eds.), *Numerical Methods for Differential Equations, Optimization, and Technological Problems*, Computational Methods in Applied Sciences 27,
DOI 10.1007/978-94-007-5288-7_24,

and visco-plastic parts and the transition behaviour is obtained using a stress dependent damage potential. The basic features of the model are discussed.

24.2 Thermodynamic Formulation

The constitutive model is derived using a thermodynamic formulation, in which the material behaviour is described completely through the Helmholz free energy and the dissipation potential in terms of the variables of state and dissipation and considering that the Clausius-Duhem inequality is satisfied [6].

The Helmholtz free energy

$$\psi = \psi(\boldsymbol{\varepsilon}_\mathrm{e}, \mathbf{D})$$

is assumed to be a function of the elastic strains, $\boldsymbol{\varepsilon}_\mathrm{e}$, and the damage vector $\mathbf{D}$. Assuming small strains, the total strain can be additively decomposed into elastic and inelastic strains $\boldsymbol{\varepsilon}_\mathrm{i}$ as $\boldsymbol{\varepsilon} = \boldsymbol{\varepsilon}_\mathrm{e} + \boldsymbol{\varepsilon}_\mathrm{i}$.

The Clausius-Duhem inequality, in the absence of thermal effects, is formulated as

$$\gamma \geq 0, \qquad \gamma = -\rho\dot{\psi} + \boldsymbol{\sigma} : \dot{\boldsymbol{\varepsilon}}, \tag{24.1}$$

where ρ is the material density. As usual in the solid mechanics, the dissipation potential

$$\varphi = \varphi(\boldsymbol{\sigma}, \mathbf{Y})$$

is expressed in terms of the thermodynamic forces $\boldsymbol{\sigma}$ and $\mathbf{Y}$ dual to the fluxes $\dot{\boldsymbol{\varepsilon}}_\mathrm{i}$ and $\dot{\mathbf{D}}$, respectively. The dissipation potential is associated with the power of dissipation, γ, such that

$$\gamma = \frac{\partial \varphi}{\partial \boldsymbol{\sigma}} : \boldsymbol{\sigma} + \frac{\partial \varphi}{\partial \mathbf{Y}} \cdot \mathbf{Y}. \tag{24.2}$$

Using the definition (24.2), Eq. $(24.1)_2$, and defining that $\rho \partial \psi / \partial \mathbf{D} = -\mathbf{Y}$, results in the equation

$$\left(\boldsymbol{\sigma} - \rho \frac{\partial \psi}{\partial \boldsymbol{\varepsilon}_\mathrm{e}}\right) : \dot{\boldsymbol{\varepsilon}}_\mathrm{e} + \left(\dot{\boldsymbol{\varepsilon}}_\mathrm{i} - \frac{\partial \varphi}{\partial \boldsymbol{\sigma}}\right) : \boldsymbol{\sigma} + \left(\dot{\mathbf{D}} - \frac{\partial \varphi}{\partial \mathbf{Y}}\right) \cdot \mathbf{Y} = 0. \tag{24.3}$$

Then, if (24.3) holds for any evolution of $\dot{\varepsilon}_\mathrm{e}$, σ and Y, the inequality (24.1) is satisfied and the following relevant constitutive relations are obtained:

$$\boldsymbol{\sigma} = \rho \frac{\partial \psi}{\partial \boldsymbol{\varepsilon}_\mathrm{e}}, \qquad \dot{\boldsymbol{\varepsilon}}_\mathrm{i} = \frac{\partial \varphi}{\partial \boldsymbol{\sigma}}, \qquad \dot{\mathbf{D}} = \frac{\partial \varphi}{\partial \mathbf{Y}}. \tag{24.4}$$

24.3 Particular Model

In the present formulation, the Helmholtz free energy, ψ, is a function depending on the symmetric second-order strain tensor $\boldsymbol{\varepsilon}_\mathrm{e}$ and the damage vector $\mathbf{D}$. The integrity basis thus consists of the following six invariants:

$$\begin{aligned} &I_1 = \operatorname{tr}\boldsymbol{\varepsilon}_\mathrm{e}, \qquad I_2 = \frac{1}{2}\operatorname{tr}\boldsymbol{\varepsilon}_\mathrm{e}^2, \qquad I_3 = \frac{1}{3}\operatorname{tr}\boldsymbol{\varepsilon}_\mathrm{e}^3, \qquad I_4 = \|\mathbf{D}\|, \\ &I_5 = \mathbf{D}\cdot\boldsymbol{\varepsilon}_\mathrm{e}\cdot\mathbf{D}, \qquad I_6 = \mathbf{D}\cdot\boldsymbol{\varepsilon}_\mathrm{e}^2\cdot\mathbf{D}. \end{aligned} \tag{24.5}$$

A particular expression for the free energy, describing the elastic material behaviour with the directional reduction effect due to damage, is given by [8]

$$\begin{aligned} \rho\psi = (1-I_4)\left(\frac{1}{2}\lambda I_1^2 + 2\mu I_2\right) + H\big(\sigma^\perp\big)\frac{\lambda\mu}{\lambda+2\mu}\big(I_4 I_1^2 - 2I_1 I_5 I_4^{-1} + I_5^2 I_4^{-3}\big) \\ + \big(1-H\big(\sigma^\perp\big)\big)\left(\frac{1}{2}\lambda I_4 I_1^2 + \mu I_5^2 I_4^{-3}\right) + \mu\big(2I_4 I_2 + I_5^2 I_4^{-3} - 2I_6 I_4^{-1}\big), \end{aligned} \tag{24.6}$$

where λ and μ are the Lamé parameters, H is the Heaviside step function and

$$\sigma^\perp = \lambda I_1 + 2\mu\hat{\mathbf{D}}\cdot\boldsymbol{\varepsilon}_\mathrm{e}\cdot\hat{\mathbf{D}}, \quad \text{and} \quad \hat{\mathbf{D}} = \mathbf{D}/I_4. \tag{24.7}$$

To model the ductile-to-brittle transition due to an increasing strain rate, the dissipation potential is decomposed into the brittle damage part, φ_d, and the ductile viscoplastic part, φ_vp, as

$$\varphi(\boldsymbol{\sigma}, \mathbf{Y}) = \varphi_\mathrm{d}(\mathbf{Y})\varphi_\mathrm{tr}(\boldsymbol{\sigma}) + \varphi_\mathrm{vp}(\boldsymbol{\sigma}), \tag{24.8}$$

where the transition function, φ_tr, deals with the change in the mode of deformation when the strain rate $\dot{\boldsymbol{\varepsilon}}_\mathrm{i}$ increases. Applying an overstress type of viscoplasticity [2, 13, 14] and the principle of strain equivalence [11, 12], the following choices are made to characterize the inelastic material behaviour:

$$\varphi_\mathrm{d} = \frac{1}{2r+2}\frac{Y_\mathrm{r}^2}{\tau_\mathrm{d}(1-I_4)}H(\varepsilon_1 - \varepsilon_\mathrm{tresh})\left(\frac{(\mathbf{Y}-\mathbf{Y}_0)\cdot\mathbf{M}\cdot(\mathbf{Y}-\mathbf{Y}_0)}{Y_\mathrm{r}^2}\right)^{r+1}, \tag{24.9}$$

$$\varphi_\mathrm{tr} = \frac{1-I_4}{pn}\left[\frac{1}{\tau_\mathrm{vp}\eta}\left(\frac{\bar{\sigma}}{(1-I_4)\sigma_\mathrm{r}}\right)^p\right]^n, \tag{24.10}$$

$$\varphi_\mathrm{vp} = \frac{1}{p+1}\frac{(1-I_4)\sigma_\mathrm{r}}{\tau_\mathrm{vp}}\left(\frac{\bar{\sigma}}{(1-I_4)\sigma_\mathrm{r}}\right)^{p+1}, \tag{24.11}$$

where the parameters τ_d, r and n are associated with the damage evolution, and the parameters τ_vp and p with the visco-plastic flow. In addition, η denotes the inelastic transition strain rate and $\mathbf{Y}_0 = \beta Y_\mathrm{r}\mathbf{n}$, where β is a small number, acts as a seed for the

damage evolution, and $\mathbf{n}$ is the eigenvector of the elastic strain tensor corresponding to the largest principal strain ε_1. The damage threshold strain is $\varepsilon_{\text{tresh}}$. The direction of the damage vector is defined through the tensor $\mathbf{M} = \mathbf{n} \otimes \mathbf{n}$ where $\otimes$ denotes the tensor product. The relaxation times τ_{d} and τ_{vp} have the dimension of time and the exponents r, $p \geq 0$ and $n \geq 1$ are dimensionless. $\bar{\sigma}$ is a scalar function of stress, e.g. the effective stress $\sigma_{\text{eff}} = \sqrt{3J_2}$, where J_2 is the second invariant of the deviatoric stress. The reference values Y_{r} and σ_{r} can be chosen arbitrarily, and they are used to make the expressions dimensionally reasonable. Since only isotropic elasticity is considered, the reference value Y_{r} has been chosen as

$$Y_{\text{r}} = \sigma_{\text{r}}^2 / E, \tag{24.12}$$

where E is the Young modulus.

Making use of (24.4), the choices (24.6)–(24.11) yield the desired constitutive equations.

24.4 On the Integration Algorithms

There are many different algorithms for the integration of inelastic constitutive models. However, the fully implicit backward Euler scheme seems to be the most popular, although it is only first-order accurate [15–17]. In practical problems, especially in those of creep and viscoplasticity, the time steps are often large, several magnitudes larger than the critical time step of some explicit methods, e.g. the forward Euler method. Therefore, the integrator should be unconditionally stable and sufficiently accurate for large time steps.

As shown in [10], the asymptotic convergence rate does not necessarily reflect high accuracy outside the asymptotic range, which usually means step sizes smaller than the critical time step of the explicit Euler method. For large time steps, the first-order accurate backward Euler method seems to be more accurate than many higher-order schemes. Therefore, an integrator for inelastic constitutive models should be at least [9, 10]:

- L-stable
- and for $\dot{\sigma} + \lambda\sigma = 0$, $\lambda =$ constant, the stability function should be
  - strictly positive, and
  - monotonous with respect to time step.

It is obvious that the standard backward Euler scheme fulfils these requirements.

When damage is included in the constitutive model, behaviour of the solution of the governing evolution equations is completely different from that of viscous and plastic solutions. Solutions of problems in creep, plasticity, and viscoplasticity are diffusive and decay exponentially with time whereas damage produces a reactive type of solutions growing exponentially with time [3].

24.4.1 Standard Backward Euler Scheme

For rate-dependent solids implicit time integrators are preferable. In this study, the backward Euler scheme is used to integrate the constitutive model at the integration point level. Although the backward Euler scheme is asymptotically only first-order accurate, it has good accuracy properties for large, practically relevant time steps [10].

Using matrix notation, the constitutive model (24.4) is rewritten in the form

$$\dot{\boldsymbol{\sigma}} = \mathbf{f}_\sigma(\boldsymbol{\sigma}, \mathbf{D}), \tag{24.13}$$

$$\dot{\mathbf{D}} = \mathbf{f}_D(\boldsymbol{\sigma}, \mathbf{D}) \tag{24.14}$$

such that

$$\mathbf{f}_\sigma(\boldsymbol{\sigma}, \mathbf{D}) = \mathbf{C}(\dot{\boldsymbol{\varepsilon}} - \dot{\boldsymbol{\varepsilon}}_\mathrm{i}) + \frac{\partial \mathbf{C}}{\partial \mathbf{D}} \mathbf{C}^{-1} \boldsymbol{\sigma}, \tag{24.15}$$

$$\mathbf{f}_D(\boldsymbol{\sigma}, \mathbf{D}) = -\frac{\varphi_\mathrm{tr} H(\varepsilon_1 - \varepsilon_\mathrm{tresh})}{\tau_\mathrm{d}(1 - I_4)} \left(\frac{(\mathbf{Y} - \mathbf{Y}_0) \cdot \mathbf{M} \cdot (\mathbf{Y} - \mathbf{Y}_0)}{Y_\mathrm{r}^2} \right)^r, \tag{24.16}$$

where the elastic stress is $\boldsymbol{\sigma}_\mathrm{e} = \mathbf{C} : \boldsymbol{\varepsilon}_\mathrm{e}$, and the elastic constitutive matrix $\mathbf{C}$ of a damaged solid can be most conveniently written using the tensor component representation

$$\begin{aligned} C_{ijkl} = {} & \lambda\big(1 - \tilde{\lambda} I_4 H\big(\sigma^\perp\big)\big)\delta_{ij}\delta_{kl} + 2\mu\big[\delta_{ik}\delta_{jl} - \tilde{\lambda} I_4 H\big(\sigma^\perp\big)(\delta_{ij}\hat{D}_i\hat{D}_j + \hat{D}_i\hat{D}_j\delta_{kl})\big] \\ & + 2\mu\big[2 + (\tilde{\lambda} - 1)H\big(\sigma^\perp\big)\big] I_4 \hat{D}_i \hat{D}_j \hat{D}_k \hat{D}_l \\ & - 2\mu I_4(\delta_{il}\hat{D}_j\hat{D}_k + \delta_{jk}\hat{D}_i\hat{D}_l), \end{aligned} \tag{24.17}$$

where $\tilde{\lambda} = \lambda/(\lambda + 2\mu)$.

Applying the backward Euler scheme and the Newton linearisation method to the evolution equations (24.13) and (24.14) results in the linear system of equations[1]

$$\begin{bmatrix} \mathbf{H}_{11} & \mathbf{H}_{12} \\ \mathbf{H}_{21} & \mathbf{H}_{22} \end{bmatrix} \begin{Bmatrix} \delta\boldsymbol{\sigma} \\ \delta\mathbf{D} \end{Bmatrix} = \Delta t \begin{Bmatrix} \mathbf{f}_\sigma \\ \mathbf{f}_D \end{Bmatrix} - \begin{Bmatrix} \Delta\boldsymbol{\sigma} \\ \Delta\mathbf{D} \end{Bmatrix}, \tag{24.18}$$

where

$$\mathbf{H}_{11} = \mathbf{I} - \Delta t \frac{\partial \mathbf{f}_\sigma}{\partial \boldsymbol{\sigma}}, \qquad \mathbf{H}_{12} = -\Delta t \frac{\partial \mathbf{f}_\sigma}{\partial \mathbf{D}},$$

$$\mathbf{H}_{21} = -\Delta t \frac{\partial \mathbf{f}_D}{\partial \boldsymbol{\sigma}}, \qquad \mathbf{H}_{22} = 1 - \Delta t \frac{\partial \mathbf{f}_D}{\partial \mathbf{D}}.$$

[1]The symbols Δ and δ refer to incremental and iterative values, $\boldsymbol{\sigma}_n^{i+1} = \boldsymbol{\sigma}_n^i + \delta\boldsymbol{\sigma}_n^i$, $\Delta\boldsymbol{\sigma}_n^i = \boldsymbol{\sigma}_n^i - \boldsymbol{\sigma}_{n-1}$, where the sub- and superscripts refer to step and iteration numbers, respectively.

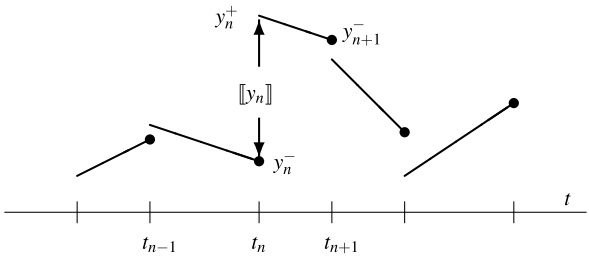

Fig. 24.1 The discontinuous Galerkin method, dG(1); notation

The algorithmic tangent matrix, i.e. the Jacobian of the algorithmic stress-strain relation has the simple form

$$\mathbf{C}^{\mathrm{ATS}} = \widetilde{\mathbf{H}}_{11}^{-1}\mathbf{C}, \tag{24.19}$$

where

$$\widetilde{\mathbf{H}}_{11} = \mathbf{H}_{11} - \mathbf{H}_{12}\mathbf{H}_{22}^{-1}\mathbf{H}_{21}.$$

As it can be seen, the Jacobian matrix is in general nonsymmetric due to the damage. The algorithmic tangent matrix is a necessity for the Newton method to obtain asymptotically quadratic convergence of the global equilibrium iterations.

24.4.2 The Discontinuous Galerkin Method

Rewrite the evolution equations (24.13) in the form

$$\dot{\mathbf{y}} = \mathbf{f}(\mathbf{y}), \tag{24.20}$$

where $\mathbf{y} = [\boldsymbol{\sigma}^T, \mathbf{D}^T]^T$ and $\mathbf{f} = [\mathbf{f}_\sigma^T, \mathbf{f}_D^T]^T$. The discontinuous Galerkin method of degree q can be stated as follows [4]. For a given time interval $I_n = (t_n, t_{n+1}]$ find $\mathbf{y}$ (polynomial of degree q) such that

$$\int_{I_n} \big(\dot{\mathbf{y}} - \mathbf{f}(\mathbf{y})\big)^T \hat{\mathbf{y}} \mathrm{d}t + [\![\mathbf{y}_n]\!]^T \hat{\mathbf{y}}_n^+ = 0. \tag{24.21}$$

For the test functions $\hat{\mathbf{y}}$, polynomials of degree q are used. The notations $\mathbf{y}_n^+$ and $\mathbf{y}_n^-$ are the limits $\mathbf{y}_n^\pm = \lim_{\varepsilon\to 0} \mathbf{y}(t_n \pm |\varepsilon|)$, $[\![\mathbf{y}_n]\!] = \mathbf{y}_n^+ - \mathbf{y}_n^-$. These notations are illustrated in Fig. 24.1.

After the Newton linearisation step, the following system of linear equations is obtained:

$$\begin{bmatrix} A_{11}\mathbf{I} - \mathbf{M}_{11} & A_{12}\mathbf{I} - \mathbf{M}_{12} \\ A_{21}\mathbf{I} - \mathbf{M}_{21} & (1 + A_{22})\mathbf{I} - \mathbf{M}_{22} \end{bmatrix}^i \begin{Bmatrix} \delta\mathbf{y}^- \\ \delta\mathbf{y}^+ \end{Bmatrix}$$
$$= \begin{Bmatrix} \mathbf{r}_1 \\ \mathbf{r}_2 \end{Bmatrix}^i - \begin{bmatrix} A_{11}\mathbf{I} & A_{12}\mathbf{I} \\ A_{21}\mathbf{I} & A_{22}\mathbf{I} \end{bmatrix} \begin{Bmatrix} \mathbf{y}^- \\ \mathbf{y}^+ \end{Bmatrix}^i - \begin{Bmatrix} \mathbf{0} \\ \mathbf{y}_n^{+i} - \mathbf{y}_n^- \end{Bmatrix}, \tag{24.22}$$

where

$$A_{ij} = \int_{I_n} N_i \dot{N}_j \mathrm{d}t, \qquad \mathbf{M}_{ij} = \int_{I_n} N_i \frac{\partial \mathbf{f}}{\partial \mathbf{y}} N_j \mathrm{d}t, \qquad \mathbf{r}_i = \int_{I_n} N_i \mathbf{f} \mathrm{d}t,$$

and N_i's are the linear interpolation functions $N_1 = (t - t_n)/\Delta t$, $N_2 = 1 - (t - t_n)/\Delta t$, which can be collected into a row vector $\mathbf{N} = [N_1, N_2]$. When the Newton iteration is converged after the k-th iteration, then $\mathbf{y}^-_{n+1} = (\mathbf{y}^-)^k$.

Partitioning the unknowns in the vector $\mathbf{y}$ as $\mathbf{y} = [(\boldsymbol{\sigma}^-)^T, (\boldsymbol{\sigma}^+)^T, \tilde{\mathbf{D}}^T]^T$, where $\tilde{\mathbf{D}} = [\mathbf{D}^{-T}, \mathbf{D}^{+T}]^T$, the coefficient matrix on the right-hand side of (24.22) can be written as

$$\mathbf{J}_{\mathrm{dG(1)}} = \begin{bmatrix} \mathbf{B}_{11} & \mathbf{B}_{12} & \mathbf{G}_{1D} \\ \mathbf{B}_{21} & \mathbf{I} + \mathbf{B}_{22} & \mathbf{G}_{2D} \\ \mathbf{G}_{D1} & \mathbf{G}_{D2} & \mathbf{G}_{DD} \end{bmatrix},$$

where

$$\mathbf{B}_{ij} = A_{ij}\mathbf{I} - \mathbf{M}_{\sigma ij}, \qquad \mathbf{M}_{\sigma ij} = \int_{I_n} N_i \frac{\partial \mathbf{f}_\sigma}{\partial \boldsymbol{\sigma}} N_j \mathrm{d}t,$$

$$\mathbf{G}_{iD} = -\int_{I_n} N_i \frac{\partial \mathbf{f}_\sigma}{\partial \tilde{\mathbf{D}}} \mathbf{N} \mathrm{d}t, \qquad \mathbf{G}_{Di} = -\int_{I_n} \mathbf{N}^T \frac{\partial \mathbf{f}_D}{\partial \boldsymbol{\sigma}} N_i \mathrm{d}t,$$

$$\mathbf{G}_{DD} = \tilde{\mathbf{A}} - \int_{I_n} \mathbf{N}^T \frac{\partial \mathbf{f}_D}{\partial \tilde{\mathbf{D}}} \mathbf{N} \mathrm{d}t, \qquad \tilde{\mathbf{A}} = \begin{bmatrix} A_{11}\mathbf{I} & A_{12}\mathbf{I} \\ A_{21}\mathbf{I} & (1 + A_{22})\mathbf{I} \end{bmatrix}.$$

The Jacobian of the algorithmic stress-strain relation for the dG(1) method has the form

$$\mathbf{C}^{\mathrm{ATS}} = \left(\tilde{\mathbf{B}}_{11} - \tilde{\mathbf{B}}_{12}\tilde{\mathbf{B}}_{22}^{-1}\tilde{\mathbf{B}}_{21}\right)^{-1}\left(\mathbf{I} - \tilde{\mathbf{B}}_{12}\tilde{\mathbf{B}}_{22}^{-1}\right)\mathbf{C},$$

where

$$\tilde{\mathbf{B}}_{ij} = \mathbf{B}_{ij} - \mathbf{G}_{iD}\mathbf{G}_{DD}^{-1}\mathbf{G}_{Dj}.$$

From the results of the subsequent section, it seems that the dG(1) method performs well in computing inelastic material behaviour with damage. The only drawback is that the method is twice as laborious as the backward Euler scheme. However, numerical experiments show that the dG(1) scheme allows larger time steps to get a converged solution, such that the overall computing time can be even shorter than with the backward Euler method in strongly non-linear cases.

24.5 Numerical Example

24.5.1 Uniaxial Straining

Performance of the integrators is tested for the coupled viscous-damage model described in Sect. 24.3. For simplicity, the transition function is assumed to be unity

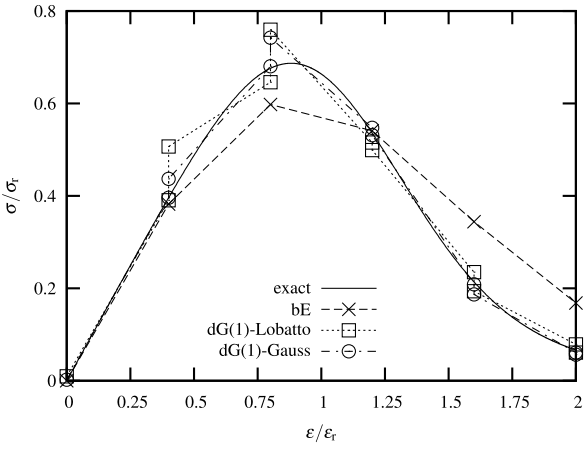

Fig. 24.2 The stress-strain relation for uniaxial constant strain-rate loading, from [3]

in this example, i.e. $\varphi_{\mathrm{tr}} \equiv 1$. The accuracy properties, when sufficiently large time steps are used, is of primary interest. The following material parameters are used: the Young modulus $E = 40\,\mathrm{GPa}$, reference stress $\sigma_{\mathrm{r}} = 20\,\mathrm{MPa}$, the viscosity parameters $\tau_{\mathrm{vp}} = 1000\,\mathrm{s}$, $\tau_{\mathrm{d}} = 0.2\,\mathrm{s}$, and the exponents $p = 4$ and $r = 1.5$. The reference value Y_{r} is chosen as in (24.12).

The stress-strain curves for an uniaxial constant strain rate $\dot{\varepsilon}_{\mathrm{c}} = 5 \times 10^{-4}\,\mathrm{s}^{-1}$ are shown in Fig. 24.2, where the true dG(1) solution, i.e. a discontinuous, piecewise linear approximation is depicted. To keep the figure readable, the end point solution values for the dG(1) methods are connected in Fig. 24.3, where the damage and inelastic strain are shown as a function of strain. Ten equal time steps are used for strain up to $4\varepsilon_{\mathrm{r}}$, thus $\Delta t = 0.4$ s. Inability of the backward Euler scheme to capture the damage evolution well is clearly visible in these figures. The "exact" solution shown in Figs. 24.2 and 24.3 is obtained by using the dG(1) method with the time step $\Delta t = 8 \times 10^{-4}$ s, resulting in 5000 steps in the range shown in Fig. 24.3. The estimated relative error for this solution is less than 10^{-5}.

24.6 Finite Element Simulations

24.6.1 Compression Test with the Scalar Damage Model

A compressed specimen ($(x, y, z) \in \Omega = (0, L) \times (0, B) \times (0, H)$, $L = 200\,\mathrm{mm}$, $B = 100\,\mathrm{mm}$, $H = 1\,\mathrm{mm}$) is analysed under a plane strain condition, as shown in Fig. 24.4. A'strain localisation into a shear band is expected to take place due to damage-induced strain softening. The horizontal displacement at the left-hand side edge is prescribed at a constant rate $\dot{u}_{\mathrm{prescibed}}$ and constrained to remain straight. A von-Mises type viscoplastic solid is used, i.e. $\bar{\sigma} = \sigma_{\mathrm{eff}}$. The constitutive parameters have the following values: the Young modulus E = 40 GPa, the Poisson ratio $\nu = 0.3$, reference stress σ_{r} = 20 MPa, the viscoplastic relaxation time

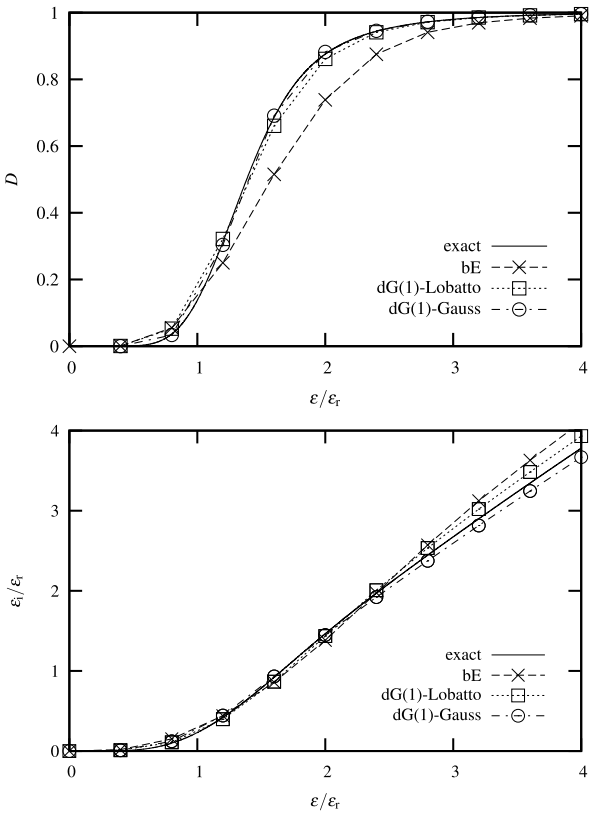

Fig. 24.3 Uniaxial constant strain-rate loading. For the dG(1) schemes, only the end points are connected [3]

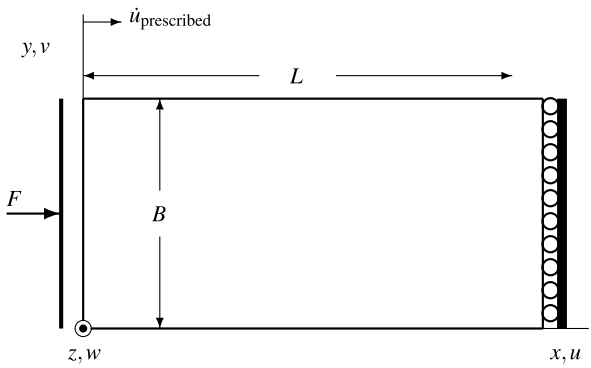

Fig. 24.4 The problem description

$\tau_{\text{vp}} = 1000\,\text{s}$, and the transition strain rate $\eta = 10^{-3}\,\text{s}^{-1}$. The exponents have the values: $p = n = 4$, and $r = 1.5$.[2]

[2]This corresponds to the same case as in [5], where the damage potential (24.9) was in the scalar case was defined in a slightly different way.

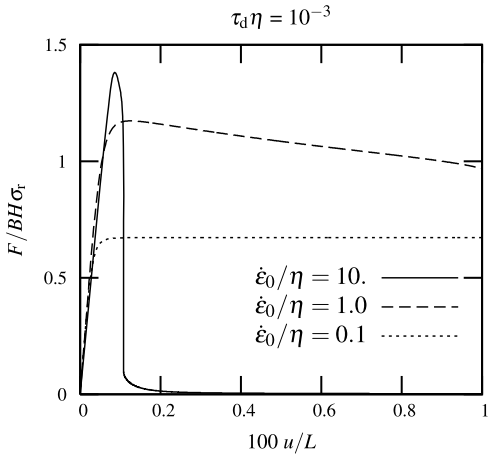

(a) The effect of the loading rate

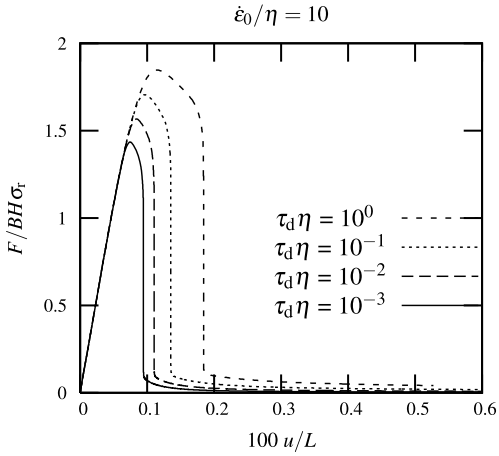

(b) The effect of the "damage viscosity" τ_d in the brittle regime

Fig. 24.5 Load-displacement curves with the mesh of 12×6 elements

Eight-node-trilinear elements with the mean dilatation formulation [7] were used in the computations, which were carried out for two different meshes, a coarse mesh of 12×6 elements and a finer mesh of 48×24 elements. To trigger the unstable localisation, an imperfection via a small patch of elements was introduced by reducing the reference stress by 5 %.

Figure 24.5 shows the load-displacement curves calculated for three different loading rates (on the upper left) and four different damage relaxation times (on the upper right) using the coarse mesh, and for both meshes considering that $\tau_d\eta = 10^{-3}$ and $\dot{\varepsilon}_0/\eta = 10$ (at the bottom). The average strain rate is defined as $\dot{\varepsilon}_0 = \dot{u}_{\text{prescribed}}/L$. In comparison to the results of pure material behaviour (Fig. 24.3,

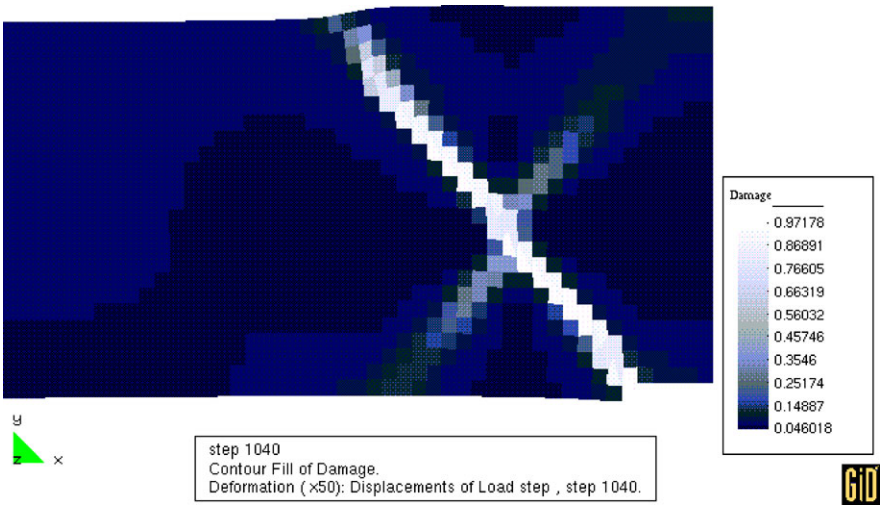

Fig. 24.6 Damage D distribution for $\dot{\varepsilon} = 10\eta$ and $\tau_d \eta = 10^{-3}$ at the end of the computation ($F = 0.618 B H \sigma_r$). A mesh of 48×24 elements. Displacements magnified 50 times

upper), the softening behaviour of the structure is much more rapid due to the localisation band.

As explained in the preceding section, a large number of time step reductions, due to diminished convergence of local iterations, had to be done during the computations, especially in the computations for the highest loading rate.

Damage distribution is shown in Fig. 24.6. It can be observed that damage bands are approximately at $\pm 45°$ angles as in the classical strain-softening von-Mises type elastoplasticity. Therefore it could be concluded that the scalar damage model is unable to capture the correct failure mode characteristic to brittle materials. It should be noted that the failure mode in tension is identical to the mode in compression with the scalar damage model. As it can be seen from the next section, to be able to predict the failure mode correctly, at least the vectorial damage model should be used.

24.6.2 Compression/Tensile Tests with the Vectorial Damage Model

The model with the vector description of damage has been implemented in the commercial finite element code ABAQUS as a user subroutine. A simple tensile test of the same specimen as in the previous example has been simulated using different loading rates, see Fig. 24.7. The same material parameters are used as with the scalar damage model simulation. The seed parameter for the damage initialisation has been $\beta = 0.025$. In Fig. 24.7(a) the load-displacement curves are shown with

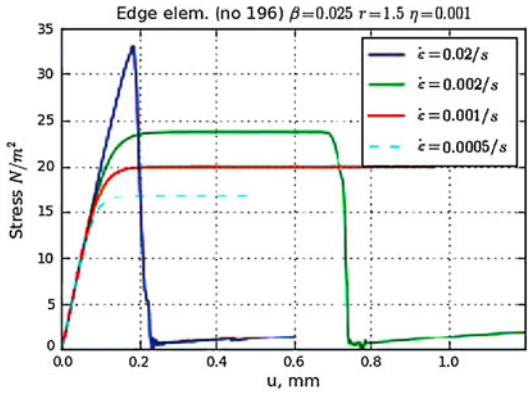

(a)

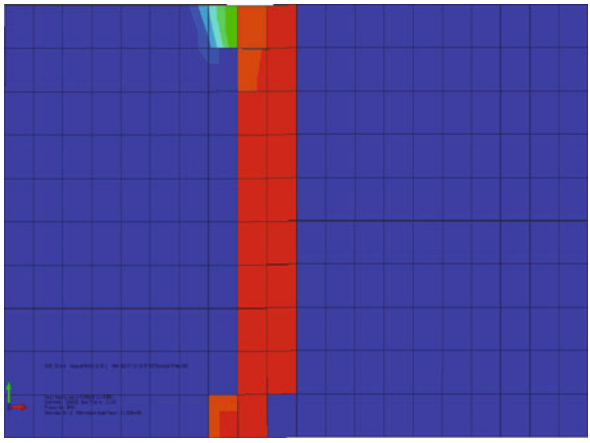

(b)

Fig. 24.7 The tensile test: stress-displacement curves with different loading rates and localisation of damage in the brittle case $\dot{\varepsilon} > 0.001\ \mathrm{s}^{-1}$

different loading rates and the failure mode is shown in Fig. 24.7(b). It can be seen that the damage is localising in an area which has a width larger than one element layer.

For the compressive loading case, the damage vectors are shown in Fig. 24.8. As it can be seen, the splitting failure mode starts to develop from the weaker elements in the mesh.

24.7 Concluding Remarks

A phenomenological constitutive model for modelling the ductile-to-brittle transition due to an increased strain rate is presented. In the present model, the dissipation potential is additively split into damage and visco-plastic parts and the transition behaviour is obtained using a stress-dependent damage potential. In this study,

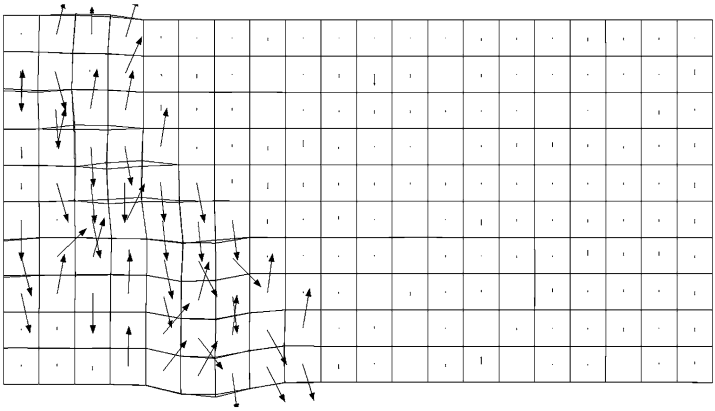

Fig. 24.8 The compression test: damage vectors **D** at the integration points on the softening regime

isotropic and vectorial damage coupled with von-Mises type viscoplastic flow are considered. However, the chosen approach allows easily an extension to more advanced damage models applicable also for realistic simulations of pressure dependent materials. To predict the correct failure mode for brittle solids, the damage cannot be described by a scalar variable. If the vectorial damage model is used, the tensile failure and splitting failure in compression can be simulated. Further investigations will be focused on the study of a material length scale.

The numerical implementation is also discussed. Due to the unstable nature of damage, the conventional backward Euler method does not perform well. Oscillations in the damage variable can result in convergence problems in the local Newton iteration at the integration point level. The discontinuous Galerkin approach seems to result in accurate results also for large time steps, and in addition, it seems to improve the convergence of the global equilibrium equations. Further studies will be directed to develop a robust integration scheme for inelastic constitutive models coupled with damage.

Acknowledgements This research has been supported in part by the Academy of Finland, decision number 121778.

References

1. Askes H, Hartikainen J, Kolari K, Kouhia R (2009) Dispersion analysis of a strain-rate dependent ductile-to-brittle transition model. In: Mäkinen R, Neittaanmäki P, Tuovinen T, Valpe K (eds) Proceedings of the 10th finnish mechanics days, University of Jyväskylä, Jyväskylä, pp 478–489
2. Duvault G, Lions L (1972) Inequalities in mechanics and physics. Springer, Berlin
3. Eirola T, Hartikainen J, Kouhia R, Manninen T (2006) Some observations on the integration of inelastic constitutive models with damage. In: Dahlblom O, Fuchs L, Persson K, Ristinmaa M, Sandberg G, Svensson I (eds) Proceedings of the 19th nordic seminar on computational mechanics, Division of Structural Mechanics, LTH, Lund University, pp 23–32

4. Eriksson K, Estep PHD, Johnsson C (1996) Computational differential equations. Studentlitteratur
5. Fortino S, Hartikainen J, Kolari K, Kouhia R, Manninen T (2006) A constitutive model for strain-rate dependent ductile-to brittle-transition. In: von Hertzen R, Halme T (eds) The IX finnish mechanics days, Lappeenranta University of Technology, Lappeenranta, pp 652–662
6. Frémond M (2002) Non-smooth thermomechanics. Springer, Berlin
7. Hughes T (1987) The finite element method. Linear static and dynamic finite element analysis. Prentice-Hall, Englewood Cliffs
8. Kolari K (2007) Damage mechanics model for brittle failure of transversely isotropic solids—finite element implementation. Tech rep 628, VTT Publications, Espoo
9. Kouhia R (2004) A time discontinuous Petrov-Galerkin method for the integration of inelastic constitutive equations. In: Neittaanmäki P, Rossi T, Majava K, Pironneau O (eds) ECCOMAS 2004 CD-ROM proceedings
10. Kouhia R, Marjamäki P, Kivilahti J (2005) On the implicit integration of rate-dependent inelastic constitutive models. Int J Numer Methods Eng 62(13):1832–1856
11. Lemaitre J (1992) A course on damage mechanics. Springer, Berlin
12. Lemaitre J, Chaboche J-L (1990) Mechanics of solid materials. Cambridge University Press, Cambridge
13. Perzyna P (1966) Fundamental problems in viscoplasticity. Advances in Applied Mechanics, vol 9. Academic Press, London
14. Ristinmaa M, Ottosen N (2000) Consequences of dynamic yield surface in viscoplasticity. Int J Solids Struct 37:4601–4622
15. Runesson K, Sture S, Willam K (1988) Integration in computational plasticity. Comput Struct 30:119–130
16. Simo J, Hughes T (1998) Computational inelasticity, 1st edn. Springer, New York
17. Wallin M, Ristinmaa M (2001) Accurate stress updating algorithm based on constant strain rate assumption. Comput Methods Appl Mech Eng 190:5583–5601